

Cluster-void degeneracy breaking: Modified gravity in the balance

Martin Sahlén^{1,2,*} and Joseph Silk^{2,3,4,5}

¹*Department of Physics and Astronomy, Uppsala University, SE-751 20 Uppsala, Sweden*

²*The Johns Hopkins University, Department of Physics and Astronomy,
3400 North Charles Street, Baltimore, Maryland 21218, USA*

³*Institut d'Astrophysique de Paris, 98 bis bd Arago, F-75014 Paris, France*

⁴*AIM-Paris-Saclay, CEA/DSM/IRFU, CNRS, Université Paris 7, F-91191 Gif-sur-Yvette, France*

⁵*BIPAC, University of Oxford, 1 Keble Road, Oxford OX1 3RH, United Kingdom*



(Received 21 December 2016; published 3 May 2018)

Combining galaxy cluster and void abundances is a novel, powerful way to constrain deviations from general relativity and the Λ CDM model. For a flat w CDM model with growth of large-scale structure parametrized by the redshift-dependent growth index $\gamma(z) = \gamma_0 + \gamma_1 z/(1+z)$ of linear matter perturbations, combining void and cluster abundances in future surveys with *Euclid* and the four-meter multiobject spectroscopic telescope could improve the figure of merit for (w, γ_0, γ_1) by a factor of 20 compared to individual abundances. In an ideal case, improvement on current cosmological data is a figure of merit factor 600 or more.

DOI: 10.1103/PhysRevD.97.103504

I. INTRODUCTION

Clusters and voids in the galaxy distribution are rare extremes of the cosmic web. As biased samples of the matter distribution, they can be used to place constraints on cosmological models. The abundances of clusters and voids are sensitive probes of dark energy [1–3], modified gravity [2,4], neutrino properties [5,6], and non-Gaussianity [7].

In earlier work [8], we derived the first statistically significant cosmological constraints from voids, showing that the joint existence of the largest known cluster and void strongly requires dark energy in the flat Λ CDM model. We also reported a powerful parameter complementarity between clusters and voids in the Λ CDM model. Here, we extend the modeling to the case where the dark energy equation of state and matter perturbation growth index are independent, free parameters. We investigate the complementarity between cluster and void abundances for constraining deviations from the general relativity (GR) + Λ CDM model, and forecast ideal-case, prior-free constraints from future surveys.

II. FIDUCIAL SURVEYS

We consider the *Euclid* Wide Survey [9] and the four-meter multiobject spectroscopic telescope (4MOST) Galaxy Redshift Survey [10]. Survey specifications are listed in Table I. For voids, we limit ourselves to the spectroscopic segment of *Euclid* and the 4MOST spectroscopic survey, for which observational systematics should

be relatively minimal (photometric redshifts can significantly distort the void shapes). We note that there is also a 4MOST cluster survey planned, which we do not consider here; our aim is to highlight the complementarity of clusters and voids, and of *Euclid* and 4MOST for void surveys.

A. Cluster selection and limiting cluster mass

The limiting cluster mass is chosen as $M_{200,c} = 8 \times 10^{13} h^{-1} M_{\odot}$ (where $M_{200,c}$ is the halo mass as defined by an overdensity of 200 above the critical density), with a constant 80% completeness [11]. A constant completeness level is not exact, but sufficiently accurate for our forecasting purposes.

B. Void selection and limiting void radius

We assume that void selection is complete for voids above the limiting radius R_{lim} (with radii defined in the galaxy field). The limiting radius is set by demanding that the void radius $R > 2R_{\text{mps}} = 2\bar{n}_{\text{gal}}^{-1/3}(z)$ [1], where $\bar{n}_{\text{gal}}(z)$ is the mean comoving galaxy number density.

We use the following prescription for *Euclid*, which provides a good fit to the galaxy densities in [12]:

TABLE I. Fiducial survey specifications.

Survey	Area [sq. deg.]	Redshift
<i>Euclid</i> clusters	15 000	0.2–2.0
<i>Euclid</i> voids	15 000	0.7–2.0
4MOST voids	12 000	0.05–1

*msahlen@msahlen.net

$$\frac{R_{\text{lim}}(z)}{h^{-1} \text{ Mpc}} = 118.272 - 334.64z + 399.22z^2 - 207.26z^3 + 40.838z^4. \quad (1)$$

For 4MOST, we assume that

$$\frac{R_{\text{lim}}(z)}{h^{-1} \text{ Mpc}} = \begin{cases} 13, & 0.05 \leq z \leq 0.5 \\ 31, & 0.5 < z \leq 0.7 \\ 15, & 0.7 < z \leq 0.8 \\ 17, & 0.8 < z \leq 0.9 \\ 42, & 0.9 < z \leq 1.0 \end{cases}, \quad (2)$$

based on the current survey plans [13].

C. Binning

We use bins in redshift $\Delta z = 0.1$, cluster mass $\Delta \log(M_{200}) = 0.2$, void radius $\Delta \log(R) = 0.1$, and void density contrast $\Delta \delta_{\text{dm}} = 0.3$ (from -1 up). This binning should accommodate expected measurement uncertainties.

III. MODEL

We predict cluster and void abundances adopting models and methodology developed in earlier work [8,14].

A. Cosmological model

We assume a flat w CDM background evolution. The primordial density perturbations follow a power-law power spectrum, and neutrinos are massless. The linear growth of perturbations is determined by the growth index $\gamma(a)$, with the linear growth rate given by [15]

$$f \equiv \frac{d \ln \delta}{d \ln a} = \Omega_{\text{m}}^{\gamma(a)}(a), \quad (3)$$

where the scale factor $a = 1/(1+z)$. The model is specified by today's values of the Hubble parameter h , mean matter density Ω_{m} , dark energy equation of state w , mean baryonic matter density Ω_{b} , statistical spread of the matter field at quasilinear scales σ_8 , scalar spectral index n_s , and growth index $\gamma(z)$. We consider (i) $\gamma(z) = \gamma_0 + \gamma_1 z/(1+z)$, (ii) $\gamma(z) = \gamma_0$ e.g. [16].

B. Number count model

We model cluster and void number counts as in [8], but with the growth of linear perturbations described by growth index $\gamma(a)$, and background by a flat w CDM model with a constant dark-energy equation of state w .

The abundance model is given by

$$\bar{N} = \iiint p(O|O_t) n[M(O_t), z] \frac{dM}{dO_t} \frac{dV}{dz} dz dO_t dO, \quad (4)$$

where O is the observable (mass, radius) for clusters or voids, O_t the true physical value of the observable O , and $M(O_t)$ the (unbiased) mass estimate of the object. The differential number density is $n(M, z)$, $p(O|O_t)$ is the probability density function (PDF) of assigning an observed value O for a true value O_t , and dV/dz is the cosmic volume element. For integrating Eq. (4), we use $M_{\text{void}} = \frac{4}{3} \pi R^3 \rho_{\text{m}}(1 + \delta_{\text{dm}})$.

C. Number density

The differential number density of objects in a mass interval dM about M at redshift z is

$$n(M, z) dM = -F(\sigma, z) \frac{\rho_{\text{m}}(z)}{M \sigma(M, z)} \frac{d\sigma(M, z)}{dM} dM, \quad (5)$$

where $\sigma(M, z)$ is the dispersion of the density field at some comoving scale $R_L = (3M/4\pi\rho_{\text{m}})^{1/3}$, and $\rho_{\text{m}}(z) = \rho_{\text{m}}(z=0)(1+z)^3$ the matter density. The expression can be written in terms of linear-theory radius R_L for voids. The multiplicity function (MF) denoted $F(\sigma, z)$ is described in the following for clusters and voids.

D. Cluster MF

The cluster (halo) MF $F_h(\sigma)$ encodes halo collapse statistics. We use the MF of Watson *et al.* [17], their Eqs. (12)–(15). Mass conversions are performed using the methods in Appendix C of [18].

E. Void MF

We employ the simulation-calibrated void MF in [1] based on a Sheth–van de Weygaert form [19],

$$F_{\text{v}} = \sqrt{\frac{2\nu}{\pi}} e^{-\nu/2}, \quad (6)$$

where $\nu = \delta_{\text{v}}^2/\sigma^2(R_L, z)$, and for which a critical density threshold $\delta_{\text{v}} = -0.45$ was derived for shell-crossed voids. We find that void-in-cloud corrections [19] are negligible for our analysis, so neglected those in Eq. (6). We generalize this prescription to other density contrasts through the spherical-expansion relationship [20],

$$\delta_{\text{v}} = c[1 - (1 + b_{\text{eff}}^{-1} \delta_{\text{dm}})^{-1/c}], \quad (7)$$

where $c = 1.594$, and we have set $\delta_{\text{m}} = b_{\text{eff}}^{-1} \delta_{\text{dm}}$ (which also defines b_{eff}). For the calibration in [1] we have $\delta_{\text{v}} = -0.45$ and $\delta_{\text{dm}} = -0.8$, which yields $b_{\text{eff}} \approx 2.44$. We then use Eq. (7) for other values of the dark-matter density contrast δ_{dm} , to convert to a linear density contrast δ_{v} to be used as the corresponding density threshold in the void MF. The void MF for (nonlinear) radius R is evaluated at corresponding linear radius R_L , which here is related as

$R/R_L = (1 + \delta_{\text{dm}})^{-1/3}$. Note that these spherical-expansion dynamics do not include any dark-energy or modified-gravity effects, but such corrections are subdominant for the model we consider [20].

While our prescription for generalizing the void MF to general density contrasts should in principle be calibrated with full simulations of the galaxy field, it is robust with respect to our conclusions (e.g. we have tested the effect of varying the value of the bias, and of a bias defined on the linear density field).

F. Scatter

We include scatter in cluster and void properties as log-normal PDFs $p(O|O_t)$ for the observable O (i.e. M_{200} or R) given its true value O_t . The intrinsic scatter between observed and true cluster mass is given by [11]

$$\sigma_{\ln M(z)}^2 = \sigma_{\ln M,0}^2 - 1 + (1+z)^{2\beta} \quad (8)$$

with $\sigma_{\ln M,0}^2 = 0.2$, $\beta = 0.125$, based on N -body simulation results. The intrinsic scatter between observed and true (spherical-equivalent) void radius is not well studied. We assume that

$$\sigma_{\ln R(z)}^2 = \sigma_{\ln R,0}^2 \quad (9)$$

with $\sigma_{\ln R,0}^2 = 0.2$, which is a reasonable first approximation given that e.g. ellipticity varies but typically is of the order 15% [21].

G. Fiducial parameters

We assume $h = 0.7$, $\Omega_m = 0.3$, $\gamma_0 = 0.545$, $\gamma_1 = 0$, $\Omega_b = 0.045$, $\sigma_8 = 0.8$, $w = -1$, $n_s = 0.96$, $\Sigma m_\nu = 0$ eV, and three neutrino species so that the early-Universe effective relativistic degrees of freedom $N_{\text{eff}} = 3.046$.

IV. LIKELIHOOD

We model the number counts of clusters and voids as Poisson distributed in each bin, and bins to be statistically independent. Hence, the log likelihood is

$$\ln \mathcal{L} = \sum_i N_i \ln \bar{N}_i - \bar{N}_i, \quad (10)$$

where N_i is the observed number of objects in bin i , and \bar{N}_i is the model prediction, Eq. (4), for the expected number of objects in the same bin.

V. COMPUTATION

We compute a Fisher matrix estimate of expected parameter constraints based on the Poisson likelihood [1]. This leads to a Fisher matrix,

$$\mathcal{F}_{mn} = \sum_i \frac{1}{\bar{N}_i} \frac{\partial \bar{N}_i}{\partial \theta_m} \frac{\partial \bar{N}_i}{\partial \theta_n}, \quad (11)$$

where \bar{N}_i is the fiducial expected number of objects in bin i and θ_m are the different model parameters under consideration. The corresponding covariance matrix $\mathcal{C} = \mathcal{F}^{-1}$. The space of eight free parameters is defined by $\{\Omega_m, \gamma_0, \gamma_1, w, \sigma_8, n_s, h, \Omega_b\}$, and we also consider the seven-parameter case where $\gamma_1 = 0$. Background evolution and linear power spectrum computations are performed using a modified version of CAMB [22].

VI. RESULTS

A. Expected numbers

We predict 5×10^5 clusters and 9×10^5 voids in the *Euclid* cluster and void surveys, and 4×10^5 voids in the 4MOST void survey. These numbers are consistent with earlier predictions [1,11].

B. Parameter constraints

The forecast ideal-case parameter constraints are shown in Fig. 1 (marginalized constraints on γ_0, γ_1 for both growth-index models) and Fig. 2 (complete set of 1D and 2D PDFs, redshift-dependent growth index only) for the

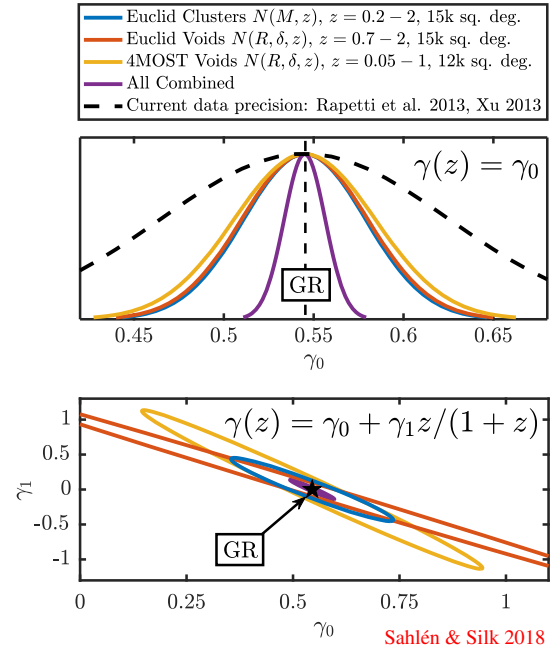


FIG. 1. Forecast marginalized PDFs for the growth index $\gamma(z)$ from cluster and void abundances in *Euclid* and 4MOST surveys, for a flat w CDM model with separate growth index $\gamma(z)$. Two different parametrizations are shown, with the two-parameter case (γ_0, γ_1) displaying 68% confidence contours. A PDF representative of current data precision [23,24] is included as a dashed line. The fiducial value of $\gamma_0 = 0.545$, $\gamma_1 = 0$ for GR + Λ CDM is also indicated.

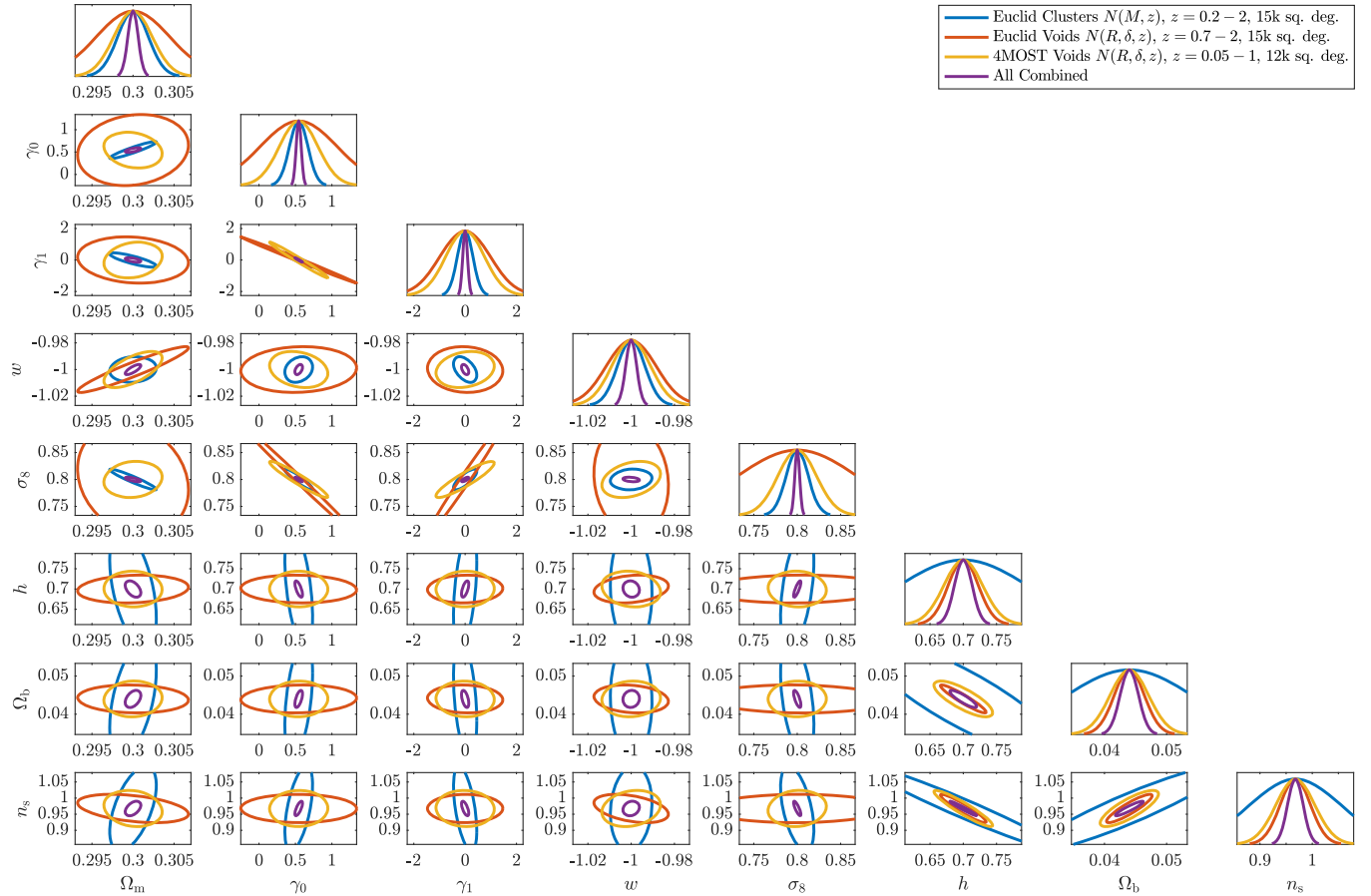


FIG. 2. Forecast 68% parameter contours, and marginal PDFs, from cluster and void abundances in future *Euclid* and 4MOST surveys, for a flat w CDM model with separate growth index $\gamma(z) = \gamma_0 + \gamma_1 z / (1 + z)$.

separate data sets and combinations thereof. Tables II and III list the forecast marginalized parameter uncertainties. In this ideal scenario, all surveys can improve substantially on current parameter uncertainties except for h , Ω_b and n_s . Hence, including data more informative on these parameters (e.g. cosmic microwave background data) will be a valuable, but here not crucial, addition.

C. Figures of merit

The figures of merit (FoM) for the dark-energy and modified-gravity parameters, defined by

$$\text{FoM} = \frac{1}{\sqrt{\det \text{cov}(\text{parameters})}}, \quad (12)$$

are listed in Table IV. Compared to current data, an improvement factor $\mathcal{O}(10^2\text{--}10^3)$ is expected for both growth-index models in this ideal case. The *Euclid* cluster survey is at least as informative (roughly) as are the combined *Euclid* + 4MOST void surveys. When all surveys are combined, a factor $\sim 4\text{--}20$ improvement in FoM is seen in comparison. With more detailed modeling of the galaxy cluster and void distributions including mass-observable

TABLE II. Forecast parameter uncertainties for growth-index model $\gamma(z) = \gamma_0 + \gamma_1 z / (1 + z)$.

Survey	$\sigma(\Omega_m)$	$\sigma(\gamma_0)$	$\sigma(\gamma_1)$	$\sigma(w)$	$\sigma(\sigma_8)$	$\sigma(n_s)$	$\sigma(h)$	$\sigma(\Omega_b)$
EC ^a	0.002	0.13	0.30	0.006	0.01	0.09	0.10	0.010
EV ^b	0.005	0.53	0.97	0.01	0.07	0.03	0.02	0.003
4V ^c	0.002	0.26	0.75	0.01	0.02	0.04	0.03	0.003
EV + 4V	0.002	0.12	0.25	0.005	0.01	0.02	0.02	0.002
All	0.0006	0.03	0.09	0.003	0.003	0.01	0.01	0.002

^a*Euclid* Clusters.

^b*Euclid* Voids.

^c4MOST Voids.

TABLE III. Forecast and current parameter uncertainties for growth-index model $\gamma(z) = \gamma_0$.

Survey	$\sigma(\Omega_m)$	$\sigma(\gamma_0)$	$\sigma(w)$	$\sigma(\sigma_8)$	$\sigma(n_s)$	$\sigma(h)$	$\sigma(\Omega_b)$
EC	0.001	0.03	0.003	0.008	0.07	0.08	0.009
EV	0.005	0.04	0.01	0.01	0.03	0.02	0.003
4V	0.002	0.04	0.01	0.01	0.04	0.03	0.003
EV + 4V	0.002	0.02	0.005	0.005	0.02	0.02	0.002
All	0.0006	0.01	0.002	0.003	0.01	0.01	0.001
Current [23,24]	0.01	0.08	0.05	0.02	0.006	0.01	0.001

scaling relations and other sources of uncertainty, the relative improvement can be expected to be greater, since such physics and systematics are mostly independent between clusters and voids. The details of this, particularly for voids, is the subject for ongoing work in the field.

D. Parameter sensitivity

Clusters.—Cluster sensitivity to cosmological parameters is described extensively in the literature, e.g. [2,26].

Voids: General.—To examine the sensitivity of void abundance to cosmological parameters, we consider the redshift-dependent growth index model and a generic survey with a fixed limiting void radius $R_{\text{lim}} = 10h^{-1}$ Mpc and galaxy bias akin to *Euclid* and 4MOST. The survey is assumed large enough to give an unbiased sample of the largest voids (sky coverage $f_{\text{sky}} \gtrsim 0.1$), and $z = 0.05$ – 2.05 .

The effects of variations in cosmological parameters on void abundance, and their statistical significance, are shown in Fig. 3. The limiting radii of the *Euclid* and 4MOST surveys are also indicated in the figure. We discuss deep voids ($\delta_{\text{dm}} \sim -0.85$) only, but the translation to medium-deep ($\delta_{\text{dm}} \sim -0.55$) or shallow ($\delta_{\text{dm}} \sim -0.25$) voids is straightforward, as Fig. 3 indicates. We illustrate the void sensitivity to cosmological parameters with the relative change

TABLE IV. Forecast and current figures of merit (FoM) for the dark-energy and modified-gravity parameters w , γ_0 and γ_1 in the two growth-index cases considered.

Survey	FoM (w, γ_0)	FoM (w, γ_0, γ_1)
EC	1.1×10^4	3.4×10^4
EV	2.6×10^3	2.6×10^3
4V	3.0×10^3	3.8×10^3
EV + 4V	1.7×10^3	4.2×10^4
All	3.9×10^4	6.6×10^5
Current	~ 300 [23,24]	$\mathcal{O}(10^2-10^3)^a$

^aEstimated based on using $\sigma(w), \sigma(\gamma_0)$ in [23] and $\sigma(\gamma_1)$ in [25]. These are upper limits on current uncertainties. These are then scaled up according to the factor differences between Tables II and III. The estimate is robust with respect to parameter correlations.

$$\Delta\chi_{i,j}^{\text{rel}}(\Delta\theta_k) \equiv \frac{\Delta\chi(R_i, z_j; \Delta\theta_k, f_{\text{sky}})}{\sqrt{\Delta\chi^2(\Delta\theta_k, f_{\text{sky}})}} \quad (13)$$

for some small, positive single-parameter change $\Delta\theta_k$ away from the fiducial model (k indexes the cosmological parameters). Here,

$$\begin{aligned} \Delta\chi(R_i, z_j; \Delta\theta_k, f_{\text{sky}}) & \\ \equiv \frac{\bar{N}_{i,j}(\theta_k + \Delta\theta_k, f_{\text{sky}}) - \bar{N}_{i,j}(\theta_k, f_{\text{sky}})}{\sqrt{\bar{N}_{i,j}(\theta_k, f_{\text{sky}})}} & \quad (14) \end{aligned}$$

is the number count change in bin i, j relative to the fiducial model, in units of the corresponding Poisson uncertainty; and $\Delta\chi^2(\Delta\theta_k, f_{\text{sky}}) = \sum_{i,j} \Delta\chi^2(R_i, z_j; \Delta\theta_k, f_{\text{sky}})$ is the total (Poisson) $\Delta\chi^2$ across all bins.

For small $\Delta\theta_k$, we approximate

$$\Delta\chi(R_i, z_j; \Delta\theta_k, f_{\text{sky}}) = \sqrt{\frac{2f_{\text{sky}}}{\bar{N}_{i,j}}} \frac{\partial \bar{N}_{i,j}}{\partial \theta_k} \Delta\theta_k. \quad (15)$$

Then, $\Delta\chi_{i,j}^{\text{rel}}$ is independent of f_{sky} and $\Delta\theta_k$ (normalizing to the same total $\Delta\chi^2$ implicitly picks some set of $\Delta\theta$'s which all separately produce the same total $\Delta\chi^2$).

The results in Fig. 3 show a few general features: (i) suppression of small voids, (ii) relative enhancement of large voids, (iii) a redshift-dependent turnover between suppression and enhancement, and (iv) variation in scale dependence. (Suppression and enhancement switch with change of sign in $\Delta\theta$.) We discuss these features in the following.

- (i) Small-scale suppression is generically produced by changes of the comoving volume. Variations in Ω_m and w will have this effect.
- (ii) Large-scale enhancement is usually accompanied by small-scale suppression. This is because these variations are all due to changes in the matter-field dispersion $\sigma(R, z)$. A positive shift $\Delta\sigma$ (due to variation in parameters affecting power spectrum or growth) effectively changes the curvature of the void

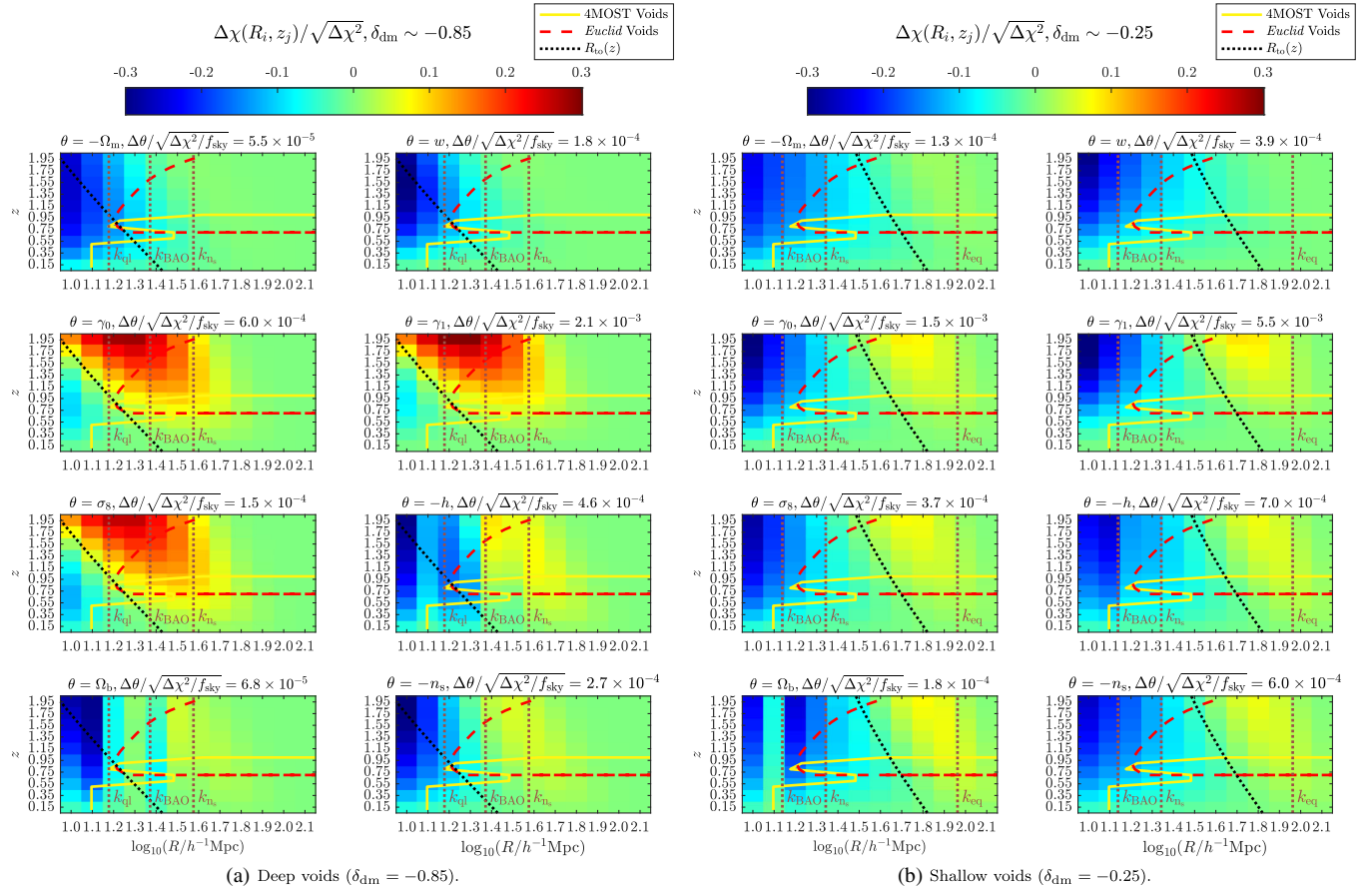


FIG. 3. Void distribution parameter sensitivity in the redshift-dependent growth index model. We assume the same fiducial cosmological and galaxy bias models as elsewhere, but consider a generic survey of deep voids with $R_{\text{lim}} = 10h^{-1}$ Mpc and $z = 0.05\text{--}2.05$, $\Delta\log_{10}(R/h^{-1} \text{ Mpc}) = 0.1$, $\Delta z = 0.2$. For each parameter, the figure shows $\Delta\chi_{i,j}^{\text{rel}}$ when that parameter *only* is varied (hence, σ_8 is kept normalized to the fiducial value at $z = 0$ when other parameters are varied). The indicated turnover radius $R_{\text{to}}(z)$ (black, dotted lines) is clearly visible in the sensitivity to power-spectrum and growth parameters. Scales related to the cosmological parameters are in brown, dotted lines ($k_{\text{qI}} = 0.13h \text{ Mpc}^{-1}$, $k_{\text{BAO}} = 0.06h \text{ Mpc}^{-1}$, $k_{n_s} = 0.05h \text{ Mpc}^{-1}$, $k_{\text{eq}} = 0.012h \text{ Mpc}^{-1}$). Note the distinct baryon acoustic oscillation signature in the Ω_b panels. The radius-redshift coverage of the surveys is also shown (4MOST, yellow solid lines; *Euclid*, red dashed lines). Some θ 's are defined with negative sign to aid comparison. Note also that $\Delta\chi_{i,j}^{\text{rel}}$ does *not* depend on f_{sky} . The normalization $\Delta\theta/\sqrt{\Delta\chi^2/f_{\text{sky}}}$ is also given for each parameter. Quantities are described further in the text.

MF, such that small scales are suppressed and large scales enhanced. This follows from noting that

$$\frac{d \ln F_v}{d \ln \sigma} = \nu - 1, \quad (16)$$

where $\nu \equiv \delta_v^2/\sigma^2(R, z)$, so small/common voids ($\nu < 1$) are suppressed and large/rare voids ($\nu > 1$) enhanced.

- (iii) The redshift-dependent turnover scale between suppression and enhancement is also explained by Eq. (16). For voids with $\nu(R, z) = 1$, $\Delta F_v/F_v \approx 0$. The turnover scale R_{to} , defined by the equation

$$\sigma(R_{\text{to}}, z) = |\delta_v| \quad (17)$$

is fairly insensitive to variations in cosmological parameters. For shallow voids $R_{\text{to}}(z = 0) \sim 65h^{-1}$ Mpc,

medium-deep voids $R_{\text{to}}(z = 0) \sim 35h^{-1}$ Mpc, and deep voids $R_{\text{to}}(z = 0) \sim 25h^{-1}$ Mpc. (Note that R_{to} depends on survey characteristics, e.g. galaxy bias.)

- (iv) Variation in scale dependence of suppression/enhancement arises primarily due to different parameters having different effects on the small-scale matter power spectrum. Small voids ($R_L \lesssim 25h^{-1}$ Mpc) are sensitive to the baryon acoustic peaks, and hence both shifts in scale ($\Omega_m h$) and power suppression ($\Omega_b h^2, n_s$) will distinctly impact the void distribution. Large voids ($R_L \gtrsim 90h^{-1}$ Mpc) are also sensitive to the turnover scale of the matter power spectrum set by matter-radiation equality ($\Omega_m h$). In addition, the relative importance of comoving volume vs density-field statistics may also play a role.

Thanks to tracer bias and the nonlinear evolution of voids, a particular tracer-defined void radius R_{tr} will correspond to a linear comoving scale,

$$R_L \approx R_{\text{tr}} \frac{(1 + b_{\text{tr}}^{-1} \delta_{\text{tr}})^{1/3}}{\beta(b_{\text{tr}})} \gtrsim \frac{R_{\text{tr}}}{2\beta(b_{\text{tr}})}, \quad (18)$$

where b_{tr} and δ_{tr} are the tracer-defined bias and density contrast, and $\beta(b_{\text{tr}}) \equiv R_{\text{tr}}/R$ relates the tracer and matter-field radii. Thus, the deepest voids correspond to the smallest scales. For $b_{\text{tr}} > 1$, $\beta(b_{\text{tr}}) > 1$, e.g. $\beta(1.4) \approx 1.2$ [8]. Hence, a survey of deep voids can probe linear comoving scales up to a factor $\sim 2\text{--}4$ smaller than the limiting void radius of the survey.

For medium-deep and shallow voids, the $\Delta\chi_{i,j}^{\text{rel}}$ patterns are qualitatively the same as in Fig. 3, but with scales shifted a factor 1.9 and 2.6, respectively.

Putting these considerations together, we suggest the following conceptual picture of how void counts constrain parameters. The *relative* numbers of deep and shallow voids at a given redshift give an effective measure of the matter power spectrum on small scales relative to large scales (i.e. its shape)—independent of growth or volume. Since the characteristic scale of the void samples change with redshift, and deep and shallow voids probe different scales in the primordial power spectrum, a wide range of scales can be constrained. Some relevant scales are indicated in Fig. 3, also showing the sensitivity to baryon acoustic oscillations. The characteristic void scale is a direct measure of the turnover radius $R_{\text{to}}(z)$, so its evolution additionally measures $\sigma(R_{\text{to}}, z)$. The *absolute* number counts can then measure the background expansion via the direct effect of Ω_m and w on cosmic volume and their indirect effect on the growth rate. The turnover radius roughly defines the boundary between volume-dominated and growth-dominated voids. The growth-dominated counts also additionally constrain $\sigma(R, z)$. This picture suggests that void counts can constrain the background expansion, shape of the power spectrum, and growth history independently.

voids: Parameters with Euclid + 4MOST.—We find that deep voids provide the strongest parameter constraints, except for Ω_m and w with *Euclid*, where shallow voids do best. Looking at Fig. 3 this is not surprising, since the sensitivity within the *Euclid* region is greater for shallow voids. However, shallow-void parameter constraints are also similar and complementary to deep voids, such that the combined constraints are tighter than the individual ones. An exception to this is γ_0, γ_1 with 4MOST, where the deep voids provide almost all constraining power.

Looking at Tables II and III, there is a difference in constraining power between the one-parameter and two-parameter growth models only in the normalization and redshift evolution of the power spectrum ($\sigma_8, \gamma_0, \gamma_1$).

This agrees well with the expectation that background expansion, power spectrum shape and growth history can be independently constrained. Indeed, the dominant degeneracy is contained within $\sigma_8(z)$.

The 4MOST survey constrains Ω_m better than *Euclid*. This derives from 4MOST containing deep voids smaller than the turnover radius (see Fig. 3). Such voids are sensitive to the growth of cosmic volume, not just growth of structure (as larger voids predominantly are). This produces degeneracy directions between Ω_m and w which rotate with redshift up to $z \sim 0.8$ (where the turnover radius exits the survey, and volume growth slows down) and settle on the growth-dominated degeneracy seen in Fig. 2. The successively rotated degeneracies, when combined, constrain Ω_m better than the growth-only constraints obtained with *Euclid*.

Differences in redshift sensitivity explains why *Euclid* and 4MOST void constraints are complementary (Fig. 2), due to different redshift coverage (despite the *Euclid* void sample being twice as large). Specifically, the redshift evolution of $\sigma(R, z)$ across the survey is much weaker in *Euclid* (5%) than in 4MOST (20%) and $\Omega_m(z)$ gets close to 1. This implies that sensitivity to this redshift evolution will be correspondingly weaker. Uncertainties on $\sigma_8, \gamma_0, \gamma_1$ should then scale roughly as $\sqrt{N_{4V}/N_{EV}} \times [\Delta\sigma_{4V}/\Delta\sigma_{EV}] \approx 2.7$ between *Euclid* and 4MOST (neglecting parameter correlations). This agrees well with Table II, where *Euclid* void uncertainties are $\sim 1.3\text{--}3.5$ times the 4MOST uncertainties on those parameters. In the constant growth-index model, this difference largely disappears thanks to breaking the $\gamma_0 - \gamma_1$ degeneracy by setting $\gamma_1 = 0$.

Medium-deep void counts add marginal additional information relative to shallow + deep void counts (adding them produces at most a 25% reduction in the standard deviation of any parameter), but may be useful for calibration/systematics or tests of scale-dependent features. The results are consistent with the finding that most voids in the baryon oscillation spectroscopic survey (BOSS) have a density contrast minimum between -0.9 and -0.6 , and radius between 20 and $40h^{-1}$ Mpc [27]. Voids that fall outside these ranges are relatively rare, with great statistical weight. Consequently, the intermediate density-contrast bin adds relatively little constraining power compared to the deep and shallow bins. The BOSS analysis, finding a 3σ discrepancy in the number of deep voids relative to the simplest allowed Λ CDM model, also independently hints that the void density-contrast distribution contains novel cosmological information.

Cluster-void complementarity.—Cluster and void number count parameter constraints are complementary for several parameters. In the redshift-dependent growth-index model, γ_0 and γ_1 are strongly correlated (Pearson correlation coefficient $\rho \sim -0.98$) regardless of data combination. However, w has varying correlation with γ_0, γ_1 in

the different surveys. In the *Euclid* void survey, the correlations are $\rho \sim -0.07$ to 0.07 . For all other survey combinations, the correlations vary between $|\rho| \sim 0.2$ – 0.5 , but complementarity still reduces the overall uncertainty.

In the constant growth-index model, the parameters w and γ_0 are weakly correlated. For the individual surveys, $\rho \sim -0.28$ to 0.28 . For the combined *Euclid* + 4MOST void surveys, $\rho = -0.09$, and for all surveys combined $\rho = 0.13$. For current data constraints, $\rho \sim -0.6$ [23,24].

Complementary parameter degeneracies arise between clusters and voids, because they have different sensitivity to structure growth vs volume expansion with redshift, comoving linear scales, and orthogonal sensitivities between matter dispersion σ and Ω_m ; see Sec. 4.5 of [8]. While *Euclid* clusters are better, separately, at constraining structure growth, the void samples are better at constraining the shape of the matter power spectrum.

E. Systematics

We do not explicitly marginalize over any systematics, but have included a net effect on number counts through statistical scatter in cluster masses and void radii. The value of this scatter is assumed to be known in the forecasts, since our purpose is to establish an ideal-case limit. In the case of voids, the expected value of this scatter is not well known, but we consider only spectroscopic data to limit photometric shape distortions. It could arise due to e.g. intrinsic ellipticity, projection and Alcock-Paczynski effects, and redshift-space distortion. We also expect linear voids to have more irregular shapes than nonlinear voids, so scatter should vary with density contrast and redshift. The impact of these effects is a subject for further study; some also contain additional cosmological information. Since shallow + deep voids contain most of the cosmological information of a void-count survey, medium-deep voids could potentially be used to self-calibrate void surveys.

Our void MF is a rough approximation, suited to this proof of concept. Accurate theoretical predictions based on large-scale simulations including nonlinear modified gravity effects, detailed void characteristics, selection methods, and survey specifications are required for detailed forecasts and future real analyses. The detailed completeness in R and δ , and sources of bias such as survey boundary effects [27,28], all require further study.

Cluster samples can suffer bias due to poor mass calibration and scaling relations, skewed redshift estimates, poorly understood selection, or MF modeling, but these issues are not expected to prevent percent-level cluster cosmology with e.g. *Euclid* [11].

Ultimately, combining clusters and voids (in conjunction also with e.g. cosmic microwave background data) will help limit the impact of systematics since they, as shown here, are relatively independent probes.

VII. CONCLUSION

We find that shallow + deep voids contain almost all the cosmological information of void counts, unless models with e.g. additional scale dependence are considered. Medium-deep voids should, nonetheless, be useful for survey self-calibration. Combined constraints from voids of different depth help break degeneracies, such that background expansion, growth rate of structure, and power spectrum can be estimated fairly independently of each other.

Combining parameter constraints from cluster and void abundances in future surveys could ideally constrain deviations from GR + Λ CDM on cosmological scales to percent level. The combination can improve the dark-energy/modified-gravity figures of merit a factor of 20 or more relative to individual abundances, and ideally a factor 600+ relative to current cosmological data. This is due to clusters and voids having complementary redshift sensitivity to growth of structure vs volume expansion, and voids probing the matter power spectrum more directly and across a wider range of scales than clusters do. Void surveys are sensitive to linear comoving scales up to a factor 2–4 smaller than their limiting radius, and can cover the full range in scale from matter-radiation equality turnover $k_{\text{eq}} \sim 0.01h \text{ Mpc}^{-1}$, through baryon acoustic peaks $k_{\text{BAO}} \sim 0.06h \text{ Mpc}^{-1}$, to the cluster quasilinear regime $k_{\text{ql}} \sim 0.1h \text{ Mpc}^{-1}$. The statistical power is independent of data from the cosmic microwave background, and hence can provide a precise and independent late-Universe probe of the power spectrum of density fluctuations (but cosmic microwave background data will improve constraints).

Including additional statistics (e.g. correlation functions) and properties (e.g. measurements of cluster masses, void/cluster density profiles, gravitational lensing, ellipticities) of the void and cluster distributions should improve on this significantly. The ongoing development of void cosmology carries great potential to provide added value to current and future large-area surveys for constraining deviations from the cosmological concordance model, at low or no additional cost.

ACKNOWLEDGMENTS

We thank Tom Kitching, Brice Ménard and Johan Richard for helpful input, and the anonymous referees for good suggestions. M.S. thanks the Department of Physics & Astronomy at the Johns Hopkins University for hospitality during the preparation of this work. M.S. was supported by the Olle Engkvist Foundation (Stiftelsen Olle Engkvist Byggmästare), the U.S.-Sweden Fulbright Commission, the Helge Ax:son Johnson Foundation (Helge Ax:son Johnsons stiftelse), and the Längmanska Fund for Culture (Längmanska kulturfonden). J.S. was supported by European Research Council “Ideas” programme (Seventh Framework Programme) ERC Project No. 267117 Dark Matters (DARK) hosted by Université Pierre et Marie Curie (UPMC)–Paris 6.

- [1] A. Pisani, P. M. Sutter, N. Hamaus, E. Alizadeh, R. Biswas, B. D. Wandelt, and C. M. Hirata, *Phys. Rev. D* **92**, 083531 (2015).
- [2] S. W. Allen, A. E. Evrard, and A. B. Mantz, *Annu. Rev. Astron. Astrophys.* **49**, 409 (2011).
- [3] G. R. Blumenthal, L. N. da Costa, D. S. Goldwirth, M. Lecar, and T. Piran, *Astrophys. J.* **388**, 234 (1992).
- [4] T. Y. Lam, J. Clampitt, Y.-C. Cai, and B. Li, *Mon. Not. R. Astron. Soc.* **450**, 3319 (2015).
- [5] J. Brandbyge, S. Hannestad, T. Haugbølle, and Y. Y. Y. Wong, *J. Cosmol. Astropart. Phys.* **09** (2010) 014.
- [6] E. Massara, F. Villaescusa-Navarro, M. Viel, and P. M. Sutter, *J. Cosmol. Astropart. Phys.* **11** (2015) 018.
- [7] S. Chongchitnan and J. Silk, *Astrophys. J.* **724**, 285 (2010).
- [8] M. Sahlén, Í. Zubeldía, and J. Silk, *Astrophys. J. Lett.* **820**, L7 (2016).
- [9] R. Laureijs, J. Amiaux, S. Arduini, J. Auguères, J. Brinchmann, R. Cole, M. Cropper, C. Dabin, L. Duvet, A. Ealet *et al.*, [arXiv:1110.3193](https://arxiv.org/abs/1110.3193).
- [10] R. S. de Jong, S. Barden, O. Bellido-Tirado, J. Brynnel, C. Chiappini, É. Depagne, R. Haynes, D. Johl, D. P. Phillips, O. Schnurr *et al.*, <http://dx.doi.org/10.1117/12.2055826>.
- [11] B. Sartoris, A. Biviano, C. Fedeli, J. G. Bartlett, S. Borgani, M. Costanzi, C. Giocoli, L. Moscardini, J. Weller, B. Ascaso *et al.*, *Mon. Not. R. Astron. Soc.* **459**, 1764 (2016).
- [12] L. Amendola, S. Appleby, A. Avgoustidis, D. Bacon, T. Baker, M. Baldi, N. Bartolo, A. Blanchard, C. Bonvin, S. Borgani *et al.*, [arXiv:1606.00180](https://arxiv.org/abs/1606.00180).
- [13] 4MOST consortium (to be published).
- [14] M. Sahlén, P. T. P. Viana, A. R. Liddle, A. K. Romer, M. Davidson, M. Hosmer, E. Lloyd-Davies, K. Sabirli, C. A. Collins, P. E. Freeman *et al.*, *Mon. Not. R. Astron. Soc.* **397**, 577 (2009).
- [15] E. V. Linder, *Phys. Rev. D* **72**, 043529 (2005).
- [16] C. Di Porto, L. Amendola, and E. Branchini, *Mon. Not. R. Astron. Soc.* **423**, L97 (2012); <https://academic.oup.com/mnras/article/423/1/L97/1075124>.
- [17] W. A. Watson, I. T. Iliev, A. D'Aloisio, A. Knebe, P. R. Shapiro, and G. Yepes, *Mon. Not. R. Astron. Soc.* **433**, 1230 (2013).
- [18] W. Hu and A. V. Kravtsov, *Astrophys. J.* **584**, 702 (2003).
- [19] R. K. Sheth and R. van de Weygaert, *Mon. Not. R. Astron. Soc.* **350**, 517 (2004).
- [20] E. Jennings, Y. Li, and W. Hu, *Mon. Not. R. Astron. Soc.* **434**, 2167 (2013).
- [21] F. Leclercq, J. Jasche, P. M. Sutter, N. Hamaus, and B. Wandelt, *J. Cosmol. Astropart. Phys.* **03** (2015) 047.
- [22] U. Seljak and M. Zaldarriaga, *Astrophys. J.* **469**, 437 (1996).
- [23] D. Rapetti, C. Blake, S. W. Allen, A. Mantz, D. Parkinson, and F. Beutler, *Mon. Not. R. Astron. Soc.* **432**, 973 (2013).
- [24] L. Xu, *Phys. Rev. D* **88**, 084032 (2013).
- [25] S. Basilakos and S. Nesseris, *Phys. Rev. D* **96**, 063517 (2017).
- [26] E. S. Levine, A. E. Schulz, and M. White, *Astrophys. J.* **577**, 569 (2002).
- [27] S. Nadathur, *Mon. Not. R. Astron. Soc.* **461**, 358 (2016).
- [28] P. M. Sutter, G. Lavaux, B. D. Wandelt, D. H. Weinberg, M. S. Warren, and A. Pisani, *Mon. Not. R. Astron. Soc.* **442**, 3127 (2014).